



UNIVERSITY OF LEEDS

This is a repository copy of *Delivery of the improved BMP-2-Advanced plasmid DNA within a gene-activated scaffold accelerates mesenchymal stem cell osteogenesis and critical size defect repair.*

White Rose Research Online URL for this paper:
<http://eprints.whiterose.ac.uk/131677/>

Version: Accepted Version

Article:

Raftery, RM, Mencía-Castaño, I, Sperger, S et al. (6 more authors) (2018) Delivery of the improved BMP-2-Advanced plasmid DNA within a gene-activated scaffold accelerates mesenchymal stem cell osteogenesis and critical size defect repair. *Journal of Controlled Release*, 283. pp. 20-31. ISSN 0168-3659

<https://doi.org/10.1016/j.jconrel.2018.05.022>

© 2018 Elsevier B.V. This manuscript version is made available under the CC-BY-NC-ND 4.0 license <http://creativecommons.org/licenses/by-nc-nd/4.0/>

Reuse

This article is distributed under the terms of the Creative Commons Attribution-NonCommercial-NoDerivs (CC BY-NC-ND) licence. This licence only allows you to download this work and share it with others as long as you credit the authors, but you can't change the article in any way or use it commercially. More information and the full terms of the licence here: <https://creativecommons.org/licenses/>

Takedown

If you consider content in White Rose Research Online to be in breach of UK law, please notify us by emailing eprints@whiterose.ac.uk including the URL of the record and the reason for the withdrawal request.



eprints@whiterose.ac.uk
<https://eprints.whiterose.ac.uk/>

Delivery of the improved BMP-2-Advanced plasmid DNA within a gene-activated scaffold accelerates mesenchymal stem cell osteogenesis and critical size defect repair

Authors: Rosanne M. Raftery ¹⁻³, Irene Mencía-Castaño ¹⁻³, Simon Sperger ⁴, Gang Chen ⁵, Brenton Cavanagh ⁶, Georg Feichtinger ⁷, Heinz Redl ⁴, Ara Hacobian ⁴ and Fergal J. O'Brien ¹⁻³

***Corresponding author**

F. J. O'Brien, Tissue Engineering Research Group, Department of Anatomy, Royal College of Surgeons in Ireland, 123 St. Stephen's Green, Dublin 2, Ireland.

Tel: +353 (0)1 402 2149

Fax: +353 (0)1 402 2355

Email: fjobrien@rcsi.ie

Affiliations

¹ Tissue Engineering Research Group, Dept. of Anatomy, Royal College of Surgeons in Ireland, Dublin, Ireland

² Trinity Centre for Bioengineering, Trinity College Dublin, Dublin, Ireland

³ Advanced Materials and Bioengineering Research Centre (AMBER), RCSI and TCD, Dublin, Ireland

⁴ Ludwig Boltzmann Institute for Experimental and Clinical Traumatology/AUVA Research Center, The Austrian Cluster for Tissue Regeneration, European Institute of Excellence on Tissue Engineering and Regenerative Medicine Research (Expertissues EEIG), Vienna, Austria.

⁵ Department of Physiology and Medical Physics, Centre for the Study of Neurological Disorders, Microsurgical research and training facility (MRTF), Royal College of Surgeons in Ireland, Dublin, Ireland

⁶ Cellular and Molecular Imaging Core, Royal College of Surgeons in Ireland, Dublin, Ireland

⁷ Division of Oral Biology, School of Dentistry, Faculty of Medicine and Health, University of Leeds, United Kingdom

Declarations of interest: none

Abstract

Gene-activated scaffolds have been shown to induce controlled, sustained release of functional transgene both in vitro and in vivo. Bone morphogenetic proteins (BMPs) are potent mediators of osteogenesis however we found that the delivery of plasmid BMP-2 (pBMP-2) alone was not sufficient to enhance bone formation. Therefore, the aim of this study was to assess if the use of a series of modified BMP-2 plasmids could enhance the functionality of a pBMP-2 gene-activated scaffold and ultimately improve bone regeneration when implanted into a critical sized bone defect in vivo. A multi-cistronic plasmid encoding both BMP-2 and BMP-7 (BMP-2/7) was employed as was a BMP-2-Advanced plasmid containing a highly truncated intron sequence. With both plasmids, the highly efficient cytomegalovirus (CMV) promoter sequence was used. However, as there have been reports that the elongated factor 1- α promoter is more efficient, particularly in stem cells, a BMP-2-Advanced plasmid containing the EF1 α promoter was also tested. Chitosan nanoparticles (CS) were used to deliver each plasmid to MSCs and induced transient up-regulation of BMP-2 protein expression, in turn significantly enhancing MSC-mediated osteogenesis when compared to untreated controls ($p < 0.001$). When incorporated into a bone mimicking collagen-hydroxyapatite scaffold, the BMP-2-Advanced plasmid, under the control of the CMV promoter, induced MSCs to produce approximately 2500 μg of calcium per scaffold, significantly higher ($p < 0.001$) than all other groups. Just 4 weeks post-implantation in vivo, this cell-free gene-activated scaffold induced significantly more bone tissue formation compared to a pBMP-2 gene-activated scaffold ($p < 0.001$) as indicated by microCT and histomorphometry. Immunohistochemistry revealed that the BMP-2-Advanced plasmid accelerated differentiation of osteoprogenitor cells to mature osteoblasts, thus causing rapid healing of the bone defects. This study confirms that optimising the plasmid construct can enhance the functionality of gene-activated scaffolds and translate to accelerated bone formation in a critical sized defect.

Keywords: BMP-2; plasmid; gene delivery; gene-activated scaffold; osteogenesis; bone regeneration

1. Introduction

Bone morphogenetic proteins (BMPs) are potent mediators of osteogenesis both during bone formation and fracture healing and are the most commonly used growth factors to stimulate bone tissue formation experimentally. Indeed, both BMP-2 and BMP-7 are approved for use clinically [1-5]. However, due to the fast release of extremely high doses of recombinant protein (4.2-8.4 mg) required to enhance bone repair, there have been many reports of adverse side effects including ectopic bone formation, cytotoxicity, increased incidence of cancer as well as some reports of inadequate healing [6, 7]. Methods to control the release of these proteins and decrease the dose to more physiological levels might allow for bone repair while reducing or even eliminating the risk of side-effects. Non-viral gene therapy can be used to transfect cells with genes encoding for therapeutic proteins, such as BMPs, inducing the transfected cells to produce physiological quantities of specific protein in a controllable manner [8, 9]. Furthermore, non-viral gene delivery can ensure sustained but ultimately transient expression of the therapeutic which is an important safety aspect associated with gene therapy.

Within our laboratory, we have developed a series of gene-activated scaffold platforms capable of efficiently delivering nucleic acids to cells [10-15]. In particular, a gene-activated scaffold comprised of chitosan nanoparticles carrying plasmid DNA (pDNA) incorporated into a collagen hydroxyapatite scaffold resulted in high transfection efficiency with negligible toxicity [16] and successful transfection of host cells when implanted in vivo [17] making it highly translatable as it can be manufactured to be an off-the-shelf product. When used to deliver pDNA encoding both BMP-2 and vascular endothelial growth factor (VEGF), the gene-activated scaffold significantly accelerated bone formation over untreated and gene-free scaffold controls [17]. Interestingly, we found that the delivery of plasmid BMP-2 (pBMP-2) alone was not sufficient to enhance bone formation, thus we sought to improve the efficiency of the pBMP-2-activated scaffold by investigating the potential of modified BMP-2 encoding plasmids (Figure 1A).

When first expressed, BMPs are large inactive molecules which must be proteolytically cleaved in order to activate their specific receptors. Active BMPs exist as dimers, molecular structures with two sub-units. They can exist as homodimers, where both sub-units are identical, such as BMP-2, and also as heterodimers, where the sub-units are different, for example BMP-2/4 and BMP-2/7. While both types are active, some studies have demonstrated that heterodimers such as BMP-2/4 and BMP-2/7 are more active than homodimers [18-20]. For this reason, we sought to investigate the use of a multi-cistronic plasmid encoding BMP-2 and BMP-7 (Figure 1B) which may induce expression of BMP-2/7 heterodimers and enhance the efficiency of the gene-activated scaffold [20].

To ensure maximum efficiency of a plasmid, strategies that allow for fast transcription and more efficient translation of gene to protein can be employed [21]. Genes are made up of protein-coding regions called exons, and non-coding regions called introns which are subsequently removed by spliceosomes before mature messenger RNA (mRNA) leaves the nucleus [22, 23]. During gene transcription, introns as well as exons are copied, increasing the time and energy required to form mRNA [24]. Furthermore, during translation of mRNA to protein, codons are translated into amino acids which subsequently form proteins. Synonymous codons can have the same amino acid coding potential, however, there is evidence of preferential use within a group of synonymous codons [25]. Genes that are regularly and highly expressed are typically made up of codons that can be decoded by abundant transfer RNAs (tRNAs) while rarely expressed genes show no preference or contain codons that require rare tRNAs [26]. Therefore, by choosing codons that are used often in place of rarely used codons, referred to as codon optimisation, protein expression can be significantly enhanced [27]. In a previous study, to streamline transcription while also increasing protein production, an artificial highly truncated intron of 96 bases was inserted into the BMP-2 gene and codon optimisation was performed. This has led to faster transcription of the encoded gene and enhanced protein production and this novel plasmid is referred to as pBMP-2-Advanced [28] (Figure 1C).

Finally, the promoter sequence in a plasmid also has an effect on transcription efficiency, with the cytomegalovirus (CMV) promoter being the most commonly used due to its ability to drive high levels of mRNA transcription [29]. However, the elongation factor 1 α (EF1 α) promoter has also been shown to be an efficient alternative particularly in mesenchymal stem cells (MSCs) [30]. To test which promoter sequence was more efficient in promoting transcription of the BMP-2 gene, two different versions of the pBMP-2-Advanced plasmid were tested, containing either the CMV or the EF1 α promoter [28] (Figure 1D).

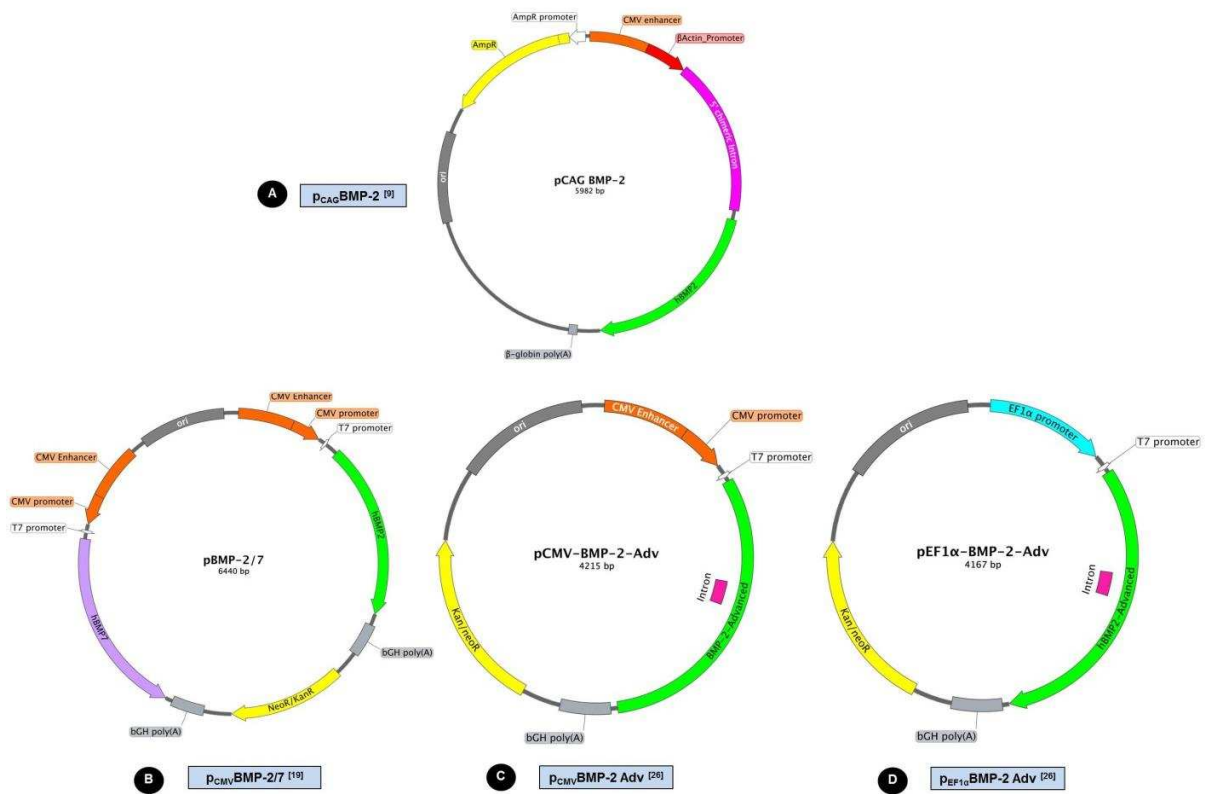


Figure 1: Plasmid maps of different BMP-2 encoding plasmids tested in this study.

The objective of this study was to investigate if using a series of modified BMP-2 plasmids could enhance the efficacy of a pBMP-2 gene-activated scaffold. Using previously optimised chitosan (CS) nanoparticles for gene delivery [16], we initially compared the modified plasmids; p_{CMV}BMP-2/7, p_{CMV}BMP-2-Adv, and p_{EF1α}BMP-2-Adv to a previously used p_{CAG}BMP-2 construct and assessed BMP-2 protein production by transfected MSCs, and BMP-2 protein functionality by quantifying MSC osteogenesis. The CS nanoparticles carrying each plasmid were then incorporated into collagen-hydroxyapatite bone-mimicking scaffolds [31], thus forming gene-activated scaffolds, and the effect of each plasmid on MSC osteogenesis was assessed. Finally, cell-free gene-activated scaffolds were implanted into critical sized calvarial defects using an established rat model and bone healing at the early time-point of four weeks was analysed to assess the ability of the gene-activated scaffolds to accelerate bone formation.

2. Materials and Methods

2.1. Comparison of BMP-2 protein production and functionality following transfection with modified BMP-2 plasmids

2.1.1 Plasmid propagation

Plasmid DNA (pDNA) encoding human bone morphogenetic protein-2, under the control of a chimeric CMV-beta actin promoter (CAG), was kindly donated by Prof. Kazihusa Bessho, Kyoto University, Japan [9] and compared to a series of BMP-2 constructs developed in the Ludwig Boltzmann Institute for Experimental and Clinical Traumatology, Vienna, namely, pBMP-2/7 [20], pBMP-2-Advanced (both under the control of the CMV promoter) and pBMP-2-Advanced under the control of the EF1 α promoter [28]. Green fluorescent protein pDNA was used as a 'non-osteogenic' control plasmid and was purchased from Lonza. All pDNA was propagated in Top10 competent E.coli cells (Invitrogen) and purified and collected following amplification using an Endotoxin free Maxi-prep kit (Qiagen, UK).

2.1.2 Chitosan-pDNA nanoparticle formulation

Oligomeric chitosan (Mw 7.3kDa; DD >97%) was supplied by Novamatrix, FMC Biopolymer, Norway. Nanoparticles were formulated by electrostatic interaction between cationic chitosan and anionic pDNA. Nanoparticles were allowed to equilibrate for 30 min at room temperature before use. The ratio of chitosan to pDNA (N/P ratio) was kept constant at 20. The pDNA dose was varied from 0.5 μ g to 10 μ g in Figure 2 and the optimal dose of 2 μ g was chosen for all further experiments [16]. For each experiment, seven groups were assessed as outlined in Table 1 below.

Table 1: Groups included in each experiment

Group	Denoted	Function
Untransfected cells	Untransfected	Control
Empty chitosan nanoparticles	CS-Empty	Control
Chitosan nanoparticles carrying pGFP (CMV promoter)	CS-p _{CMV} GFP	Control
Chitosan nanoparticles carrying pBMP-2 (CAG promoter)	CS-p _{CAG} BMP-2	Test
Chitosan nanoparticles carrying pBMP-2/7 (CMV promoter)	CS-p _{CMV} BMP-2/7	Test
Chitosan nanoparticles carrying pBMP-2-Advanced (CMV promoter)	CS-p _{CMV} BMP-2-Adv	Test

Chitosan nanoparticles carrying pBMP-2-Advanced (EF1 α promoter)

CS-p_{EF1 α} BMP-2-Adv

Test

2.1.3 Mesenchymal stem cell culture

MSCs, isolated from rat bone marrow, were expanded in Dulbecco's Modified Eagles Medium supplemented with 2% penicillin/streptomycin, 10% FBS (Labtech, UK), 1% glutamax (Biosciences, Ireland) and 1% non-essential amino acids (Biosciences, Ireland). Cells were passaged at 70-90% confluency and expanded to passage 5 for all experiments.

2.1.4 Mesenchymal stem cell transfection in 2D culture

MSCs were seeded at a density of 5×10^4 cells per well in 6 well adherent plates (Corning, Costar, Ireland) 24 h prior to transfection. Media was removed from cells 1 h prior to transfection and cells were washed in PBS (Sigma-Aldrich, Ireland) and 1 mL of OptiMEM (Gibco, Ireland) was added. Nanoparticles were made as described in Section 2.1.2 and, following complexation, OptiMEM was added in a 1:1 ratio to the nanoparticle mixture to produce the transfection medium of which 500 μ L was added to each well. After 4 h, transfection media was removed, cells were washed twice in PBS and growth media was replenished.

2.1.5 Enzyme-linked Immunosorbent Assay (ELISA)

ELISAs (R&D Systems, Biotechne, UK) were used to quantify the levels of BMP-2 expressed by cells transfected with each variant of BMP-2 plasmid as well as for all control groups. The cell culture supernatant was collected and analysed at days 1, 3, 7 and 14. Assays were carried out according to the manufacturer's instructions and the absorbance of each sample was read at 450 nm using a Varioskan Flash multimode plate reader (Fisher Scientific, Ireland). The quantity of BMP-2 protein present was deduced by calculating against a standard curve.

2.1.6 Assessment of cytotoxicity using MTT assay

MSCs were transfected as described in Section 2.1.4 and an MTT cell proliferation assay kit (Abcam) was carried out at 3 days post-transfection. This is a metabolic assay where active cellular enzymes reduce the MTT dye to formazan crystals. Briefly, 50 μ L of MTT Reagent was added to the cells in 50 μ L of serum-free media and incubated for 3 h at 37°C. After 3 h 150 μ L of MTT Solvent was added to dissolve the formazan crystals, formed by metabolically active cells, leaving behind a purple colour. The intensity of the resulting colour was read at an absorbance

of 570 nm using a reference wavelength of 630 nm using a Varioskan Flash multimode plate reader (Fisher Scientific, Ireland).

2.1.7 Preparation of cells for fluorescent imaging

pDNA was tagged with a Cy3 fluorophore using a Label IT® Nucleic acid labelling kit (Mirus Bio LLC) as per manufacturer's instructions. MSCs were transfected as described in Section 2.1.4. Five hours post-transfection, the media was removed and the cells were washed with PBS. The cells were fixed by adding 4% paraformaldehyde for 15 minutes before washing in PBS. To permeabilise the cells, 0.1% Triton X-100 solution was added before addition of a HCA cell mask green stain (Invitrogen®) was added to stain the cell membrane and left for 30 minutes before being removed and washed. Finally, Hoescht 33258 blue stain was added to stain the nucleus for 5 minutes prior to final washing in PBS. Images were acquired using an automated Olympus Scan[^]R screening microscope with a 20x/0.60 NA LUCPLFLN objective.

2.1.6 MSC osteogenesis assay

To assess if the BMP-2 protein produced by transfected cells was functional, an MSC osteogenesis assay was carried out following transfection as described in Section 2.1.3. After 5 h, OptiMEM was removed and replaced with growth media (Section 2.1.3) for three days before being changed to osteoinductive media which contained DMEM supplemented with 10% FBS, 1% penicillin/streptomycin, 10 mM β -glycerophosphate, 50 μ M ascorbic acid 2-phosphate and 100 nM dexamethasone. Media was replaced three times per week until day 14 post-transfection. Cells were harvested at days 1, 3, 7 and 14 and ALP activity and DNA content was quantified. Briefly, cells were lysed using 0.2 M sodium carbonate buffer containing 1% Triton X-100. DNA content was measured using a Quant-iT™ PicoGreen® dsDNA assay (Invitrogen, UK) according to manufacturer's protocol and DNA concentration was deduced using a standard curve. The same cell lysate was used to assess ALP activity using a SensoLyte® pNPP Alkaline Phosphatase assay kit (Cambridge Biosciences, Ireland). ALP substrate was applied to the samples and the absorbance measured at 405 nm. ALP concentration was deduced using a standard curve. Calcium content was quantified at day 14 using a Stanbio calcium assay (Calcium CPC Liquicolour, Stanbio Inc., USA). Briefly, media was removed and cells were rinsed with 1 ml of PBS. One ml of 0.5 M HCl was then added to each well and the contents of each well were scraped into microcentrifuge tubes and left to shake overnight at 4 °C. Calcium levels were then quantified according to the manufacturer's instructions against a standard curve.

2.2 Comparison of BMP-2 protein functionality following transfection with modified BMP-2 plasmids on a 3D collagen hydroxyapatite scaffold

2.2.1 Scaffold fabrication

A collagen hydroxyapatite scaffold was prepared as per patented protocol [32]; Briefly, 1.8 g of collagen (Southern Lights Biomaterials, New Zealand) was blended in 0.5 M HOAc 15,000 rpm for 90 min. Hydroxyapatite (200wt%) was dissolved separately in 0.5 M HOAc and added slowly to the collagen slurry (10 mL/h) while maintaining dispersion at 15,000 rpm. Gas was removed from the slurries using a vacuum pump prior to freeze-drying (Advantage EL, Vis-Tir Co., Gardiner NY) to a final freezing temperature of -40 °C. The scaffolds were cross linked dehydrothermally (DHT) at 105 °C for 24 h at 0.05 bar in a vacuum oven (Vacucell 22; MMM, Germany), followed by chemical cross-linking using a mixture of 6 mM N-(3-Dimethylaminopropyl)-N'-ethylcarbodiimide hydrochloride (EDC) and 5.5 mM N-Hydroxysuccinimide (NHS). Cylindrical scaffolds (10 mm diameter) were used in transfection experiments. For in vivo experiments, scaffolds were manufactured with a diameter of 8 mm and a height of 1.5 mm to fit the defect and reflect the thickness of native calvarial bone.

2.2.2 Gene-activated scaffold fabrication

Scaffolds were manufactured as described in Section 2.2.1 and nanoparticles were made as described in Section 2.1.2 as optimised previously [16]. CS-pDNA nanoparticles were formulated at an N/P ratio of 20 containing a 2 µg load of each BMP-2 plasmid. Scaffolds were hydrated in PBS before use and nanoparticles were incorporated by soak-loading onto the scaffold before MSC seeding. After 24 h the scaffolds were moved to fresh 24 well non-adherent plates in fresh expansion media for a further 2 days before being changed to osteoinductive media (Section 2.1.6).

2.2.3 Evaluating the effect of different BMP-2 plasmids on MSC osteogenesis in 3D collagen hydroxyapatite gene-activated scaffolds

Gene-activated scaffolds carrying either: CS-p_{CAG}BMP-2, CS-p_{CMV}BMP-2/7, CS-p_{CMV}BMP-2-Adv or CS-p_{EF1α}BMP-2-Adv as well as untransfected, CS-empty and CS-_{CMV}GFP controls, were fabricated as described in Section 2.2.2. After 28 days in culture, the scaffolds were removed from the wells and washed in PBS prior to further analysis. Alizarin red staining was used to investigate the level of mineralisation within the scaffolds. Samples were fixed with 10% formalin for 30 minutes and processed overnight using an automatic tissue processor (ASP300, Leica, Germany). The constructs were embedded in paraffin wax before sectioning. Sections of 5 µm

thickness were cut using a rotary microtome (Microsystems GmbH, Germany) and sections were mounted on poly-L-lysine coated glass slides (Thermo Scientific, Ireland). Samples were deparaffinised with xylene and rehydrated before being stained in 2% alizarin red for 2-3 min. Sections were then dehydrated and DPX mountant was used to attach cover slips to the slides. Digital images of all stained sections were obtained using an imaging system (AnalySIS, Nikon, Japan) in conjunction with a microscope (Olympus IX51, Olympus, Japan). Calcium content per scaffold was quantified using a Stanbio calcium assay (Calcium CPC Liquicolour, Stanbio Inc., USA) 14 and 28 days post cell seeding. Briefly, media was removed and the scaffolds were placed in 1 mL of 0.5 M HCl and left shaking overnight at 4 °C. Calcium levels were then quantified according to the manufacturer's instructions.

2.3 Efficacy of gene-activated scaffold in accelerated repair of critical sized bone defects in vivo

2.3.1 Surgical procedure

This study was conducted in accordance with protocols approved by the Research Ethics Committee of the Royal College of Surgeons in Ireland (REC 1205), and an animal licence granted by the Irish Government Department of Health (Ref. No. B100/4416) in compliance with EU directive 2010/EU/63. A total of 32 adult male Wistar rats were divided into four groups; (a) defect was left empty (n=8), denoted 'untreated'; (b) CHA scaffold alone (n=8), denoted 'gene-free scaffold'; (c) CHA scaffold containing CS-p_{CAG}BMP-2 nanoparticles (n=8), denoted 'CS-p_{CAG}BMP-2'; and (d) CHA scaffold containing CS-p_{CMV}BMP-2-Adv nanoparticles (n=8), denoted 'CS-p_{CMV}BMP-2-Adv'. The number of animals used per group to ensure a statistically powerful study was calculated using G*Power software based on previous studies using the calvarial defect model [12]. Anaesthesia was induced with intraperitoneal medetomidine hydrochloride (0.3 mg/kg) and ketamine hydrochloride (70 mg/kg) and maintained with inhalational isoflurane (0.5–2%) and oxygen. The skin of the head was shaved and cleaned using 70% ethanol and chlorhexidine before the animal was placed in the prone position on a heated aseptic operating platform prior to draping. A 3 mm sagittal skin incision over the calvarium was made and the soft tissues dissected using a blunt technique to expose the periosteum. A 7 mm trephine drill was used to create a 7 mm circular transosseous defect under constant irrigation with 0.9% NaCl. Scaffolds with a diameter of 8 mm and a height of 1.5 mm were press-fit into the defect and the periosteum and superficial connective tissue were closed in layers with 3-0 absorbable monofilament sutures (Monocryl™) and the skin was closed using a topical skin adhesive (n-butyl cyanoacrylate). Post-operatively, the animals were given a subcutaneous injection of the reversal

agent atipamezole hydrochloride (0.05 mg/kg body weight) to reverse sedation. Animals were placed in an incubator at 35 °C until fully recovered. Animals were housed (4 per cage) with ad libitum access to water, food and environmental enrichment. Antibiotics (enrofloxacin 2.5% - 10 mg/kg) were provided in the drinking water for 3 days post-surgery. At 4 weeks post-surgery, the animals were euthanised by CO₂ asphyxiation and cervical dislocation. A 20 mm x 20 mm section of the calvarium containing the defect was resected using a dental saw and the tissue was fixed for 72 h in 10% formalin before being transferred to Dulbecco's PBS.

2.4.1 Micro-computed tomography

The 20 mm x 20 mm sections of bone were analysed using micro computed tomography (μ CT). Scans were performed on a Scanco Medical 40 MicroCT system (Scanco Medical, Bassersdorf, Switzerland) with a voxel resolution of 12 μ m, a voltage of 70 kVP and a current of 112 μ A. 3D reconstruction was performed using the standard Scanco software package with a threshold of 140 in a scale from 0 to 1000, corresponding to a density of 257.99 mg HA/ccm. These settings have been optimised for the rat calvarial model previously and are routinely used within our group [12, 17, 33-36]. Volume of interest (VOI) was defined to analyse a 6 mm defect region to assess healing in the centre of the defect and to exclude any old bone at the defect edges. Repair was expressed as percentage of bone volume fraction within the defect area.

2.4.2 Histology and histomorphometry

To confirm the μ CT results, both qualitative and quantitative histology was performed on explants. The explants were first decalcified using Decalcifying Solution-Lite (Sigma-Aldrich, Ireland) for a total of 13 h before specimens were dehydrated in a graded series of ethanol solutions using an automated tissue processor, bisected and embedded in single paraffin wax blocks. Sections (7 μ m thick) were cut from the mid-portion of each sample using a rotary microtome and mounted on poly-L-lysine coated glass slides. Each section was stained with Haematoxylin and Eosin (H&E). Haematoxylin stains cell nuclei purple, eosin stains extracellular matrix pink and bone appears dark pink/red. Images of each specimen were acquired and digitised using transmitted light microscopic visualization (Nikon Microscope Eclipse 90i with NIS Elements software v3.06, Nikon Instruments Europe, The Netherlands). Quantitative analysis was performed on n=6 sections from each specimen (n=8 per group). Single blinded histomorphometric analysis was carried out in order to quantify the healing response from the H&E-stained samples. The defect margin was identified and any new bone was delineated using colour thresholding which allowed the quantification of the area of bone nucleation sites (BNS) in each section and calculation of the

mean total area of these sites per group. This was performed using an automated Image J script [37].

2.4.3 Immunohistochemistry analysis to determine osteoinductive effect of scaffolds

Immunohistochemical staining of paraffin embedded sections was carried out to assess the osteoinductive effect of the scaffolds on infiltrating endogenous cells by staining for key checkpoint markers of osteoblast differentiation from progenitor cells. Col1a1 (osteoprogenitor cells undergoing differentiation), and osteocalcin (mature osteoblasts) were used to identify cells at both stages of differentiation using rabbit IgG polyclonal antibodies (Santa Cruz Biotech., Germany). Two samples per animal were analysed (n=8). Samples were prepared for staining by deparaffinisation and rehydration, followed by heat-activated citrate-based antigen retrieval. Samples were then incubated with a 1% H₂O₂ peroxidase inhibitor (ThermoScientific, Ireland), before blocking in 5% horse serum (ThermoScientific, Ireland). Samples were then incubated at 4 °C overnight with a 1:100 dilution of each corresponding primary antibody. To complete staining, a goat IgG Vectastain Elite ABC Kit was used in combination with a DAB Substrate kit (all from Vector labs, UK) according to manufacturer's instructions. Finally, the sections were counterstained using Mayer's haematoxylin counterstaining and mounted with DPX (ThermoScientific). Digital imaging was performed using the Nikon Eclipse 90i digital microscope system and five random sections were acquired for each specimen. Image J software was utilised to quantify % area of positive DAB staining using the automated pixel saturation method as in Section 2.4.2.

2.5 Statistical analysis

Results are expressed as mean ± standard deviation. Statistics were carried out using Graphpad Prism software using a general linear model ANOVA with post-hoc analysis performed for multiple comparisons. p<0.05 values were considered statistically significant where * p<0.05, ** p<0.01 and *** p<0.001.

3. Results

3.1. Comparison of BMP-2 protein production and functionality following transfection with modified BMP-2 plasmids

To confirm the optimal pDNA dose required to elicit the highest level of protein production while simultaneously avoiding cellular toxicity, a pDNA dose response study was carried out. pDNA doses of 0.5, 1, 2, 5 and 10 µg were delivered to cells at a constant N/P ratio of 20. In Figure 2 A-E the nanoparticles (red) at each pDNA dose can be seen surrounding the cells (green) 5 h post-transfection and evidence of nanoparticle aggregation can be seen at the higher pDNA doses of 5 and 10 µg. A pDNA dose of 2 µg/well induced the highest level of BMP-2 protein production, significantly higher than all other doses, at 3 days post-transfection (Figure 2 F). Furthermore, at doses of 5 and 10 µg/well, significant cytotoxicity was observed and, likely due to the sheer number of nanoparticles binding to the cell membrane. Therefore, the optimal pDNA dose was found to be 2 µg/well at an N/P ratio of 20, confirming previously published data [16].

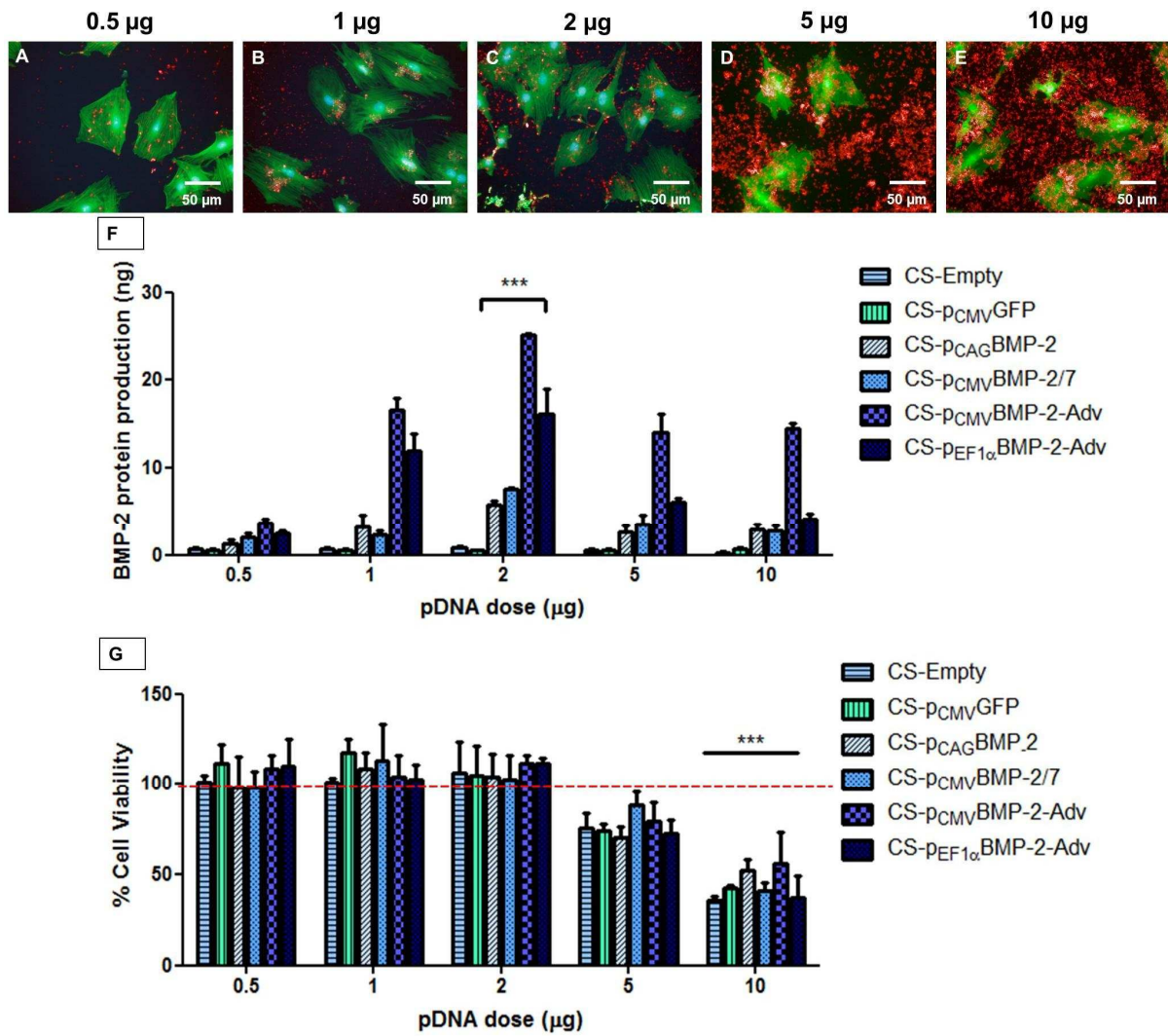


Figure 2: A pDNA dose response study to determine the optimal pDNA dose for transfection. Fluorescent microscopy images show increasing evidence of nanoparticle aggregation with increasing pDNA dose with A) 0.5 µg; B) 1 µg; C) 2 µg; D) 5 µg; and E) 10 µg. The 2 µg pDNA dose inducing the highest protein production by cells 3 days post-transfection as determined by ELISA (F) and high concentrations of pDNA (10 µg/well) induced significant cellular toxicity. Data plotted represents mean ± SD where n=3. Two-way ANOVA followed by Bonferoni post hoc analysis was performed and *** indicates p<0.001 compared to other doses in F and compared to untreated controls (represented by the dashed line) in G.

The transient expression of BMP-2 protein by cells over time was also monitored using ELISA (Figure 3) using the optimal nanoparticle formulation of N/P 20 carrying 2 µg of pDNA. As expected, there was no increase in BMP-2 protein production by cells that were either untransfected, transfected with CS-empty or CS-p_{CMV}GFP thus confirming that the CS

nanoparticles are not affecting BMP-2 production. All cells treated with a BMP-2 plasmid responded by significantly increasing BMP-2 protein production over controls at day 3 and 7 ($p < 0.05$), indicating positive transfection. The CS- $p_{CMV}BMP-2/7$ treated cells produced significantly more BMP-2 compared to cells treated with $p_{CAG}BMP-2$. Encouragingly, both BMP-2-Adv plasmids significantly enhanced BMP-2 protein production by transfected cells when compared to all other groups ($p < 0.001$), and at the earlier time-point of day 3. In particular, the $p_{CMV}BMP-2-Adv$ proved to be the most efficient plasmid for inducing BMP-2 protein production by MSCs even when compared to $p_{EF1\alpha}BMP-2-Adv$.

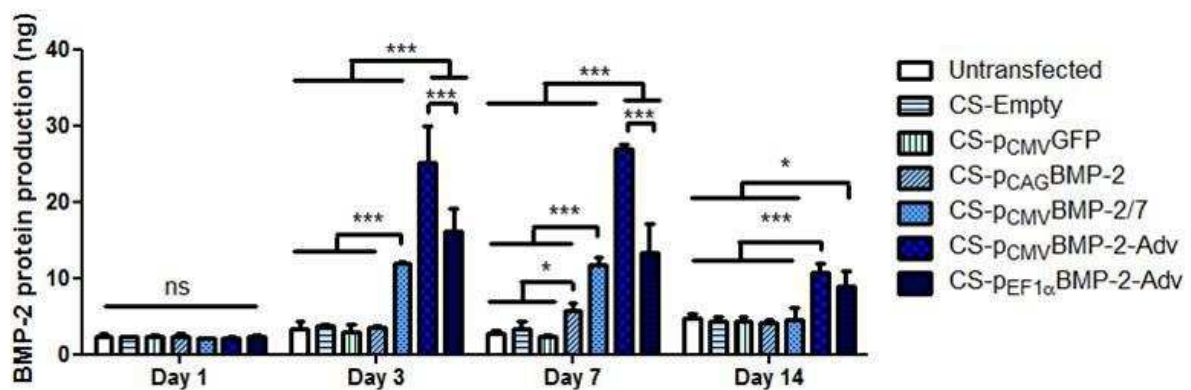


Figure 3: Assessment of BMP-2 protein production by transfected cells. Untransfected cells were compared to cells treated with CS-empty, CS- $p_{CMV}GFP$, CS- $p_{CAG}BMP-2$, CS- $p_{CMV}BMP-2/7$, CS- $p_{CMV}BMP-2-Adv$ and CS- $p_{EF1\alpha}BMP-2-Adv$. BMP-2 protein production as monitored by ELISA at day 1, 3, 7 and 14 post-transfection. Each of the four BMP-2 plasmids induced cells to produce more BMP-2 protein than controls. The $p_{CMV}BMP-2-Adv$ induced cells to produce significantly more BMP-2 protein than all other groups at days 3, 7 and 14. Data plotted represents mean \pm SD where $n=3$. Two-way ANOVA followed by Bonferroni post hoc analysis was performed and * represents $p < 0.05$ and *** represents $p < 0.001$.

To assess if the BMP-2 protein produced by transfected cells retained its osteoinductive properties, alkaline phosphatase activity was monitored at days 1, 3, 7 and 14 post-transfection. There was no increase in ALP activity in untransfected cells cultured in growth media (GM) for 14 days (Figure 4A). When untransfected cells were cultured in osteogenic media (Figure 4B), there was a significant increase in ALP activity at days 3 and 7 ($p < 0.05$) and similar levels of ALP activity were seen in cells treated with CS-empty (Figure 4C) and CS- $p_{CMV}GFP$ (Figure 4D). ALP activity was significantly increased following treatment with each BMP-2 plasmid however $p_{CMV}BMP-2-Adv$ induced the highest level of ALP activity (Figure 4G). Interestingly, ALP activity peaked at day 7 in cells transfected with CS- $p_{CAG}BMP-2$ (Figure 4E) and CS- $p_{CMV}BMP-2/7$ (Figure 3F) while

an earlier peak in ALP activity at day 3 was evident in the cells transfected with CS-p_{CMV}BMP-2-Adv and CS-p_{EF1 α} BMP-2-Adv (Figure 4G and H).

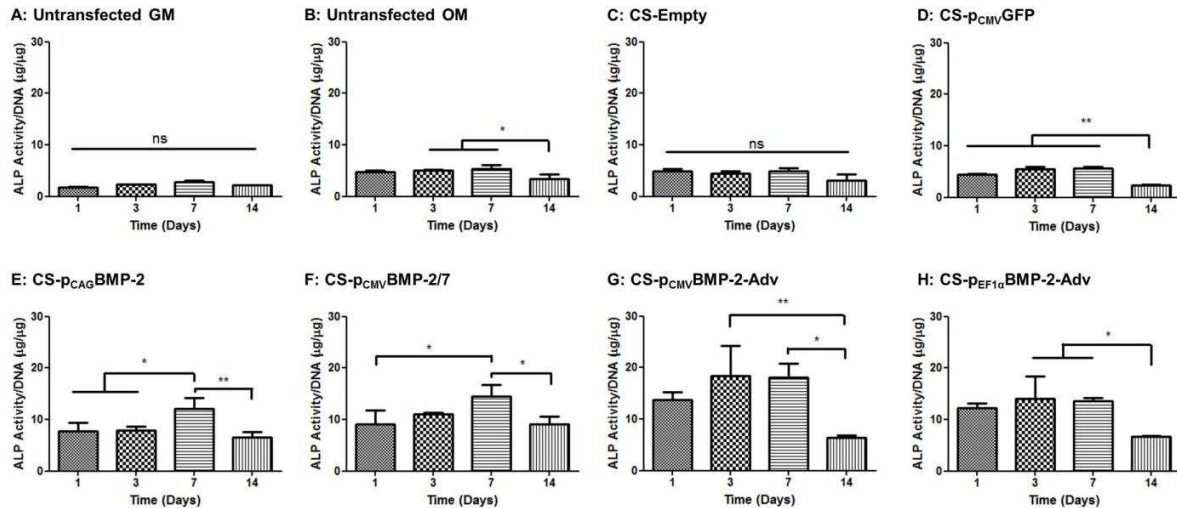


Figure 4: Effect of osteoinductive genes on MSC differentiation as measured by ALP activity. Untransfected cells in growth media (GM) (A), osteoinductive media (OM) (B) were compared to cells treated with CS-empty (C), CS-p_{CMV}GFP (D), CS-p_{CAG}BMP-2 (E), CS-p_{CMV}BMP-2/7 (F), CS-p_{CMV}BMP-2-Adv (G) and CS-p_{EF1 α} BMP-2-Adv (H), all of which were cultured in osteoinductive media. ALP activity by MSCs was measured at days 1, 3, 7 and 14 post-transfection. ALP activity was highest in cells transfected with CS-p_{CMV}BMP-2-Adv. ALP activity peaked earlier in cells treated with both pBMP-2-Adv plasmids at day 3 with a later peak in ALP activity evident in cells treated with BMP-2 and BMP-2/7 plasmids. Data plotted represents mean \pm SD where n=3. One-way ANOVA followed by Tukey post hoc analysis was performed and * represents $p < 0.05$ and ** represents $p < 0.01$.

To confirm the osteoinductive effect of the BMP-2 protein produced by cells post-transfection on MSC osteogenesis, calcium deposition by transfected cells was quantified 14 days after transfection (Figure 5). As with the ALP activity experiments (Figure 4), all cells were cultured in osteoinductive media (Section 2.1.6) from day 3 post-transfection with the exception of the untransfected GM control with GM denoting growth media. As expected, the cells in osteoinductive media (OM) deposited more calcium than the untransfected cells in GM ($p < 0.01$). Calcium deposition by the control cells - untransfected in OM, CS-Empty and CS-p_{CMV}GFP, was similar while all cells transfected with a pBMP-2 plasmid induced significantly more calcium deposition. Comparing CS-pBMP-2 transfected groups, it was evident that the CS-p_{CMV}BMP-2-Adv treated cells deposited significantly more calcium than other groups ($p < 0.001$) including the CS-p_{EF1 α} BMP-2-Adv group ($p < 0.05$).

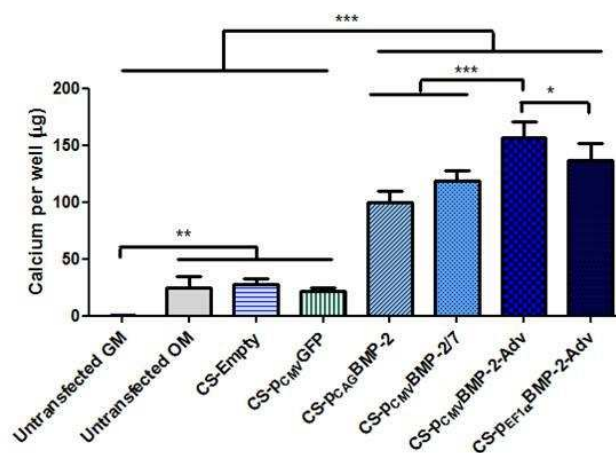


Figure 5. Effect of osteoinductive genes on MSC osteogenesis in 2D monolayer as measured by calcium deposition quantification. Untransfected cells in growth media (GM) and osteoinductive media (OM) were compared to cells treated with CS-empty, CS-p_{CMV}GFP, CS-p_{CAG}BMP-2, CS-p_{CMV}BMP-2/7, CS-p_{CMV}BMP-2-Adv and CS-p_{EF1α}BMP-2-Adv. Calcium deposition was quantified 14 days post-transfection. Each condition induced cells to produce significantly more calcium than untransfected cells in growth media. Each variant of BMP-2 plasmid induced significantly more calcium deposition than controls without a BMP-2 plasmid. The CS-p_{CMV}BMP-2-Adv transfected group induced significantly higher levels of calcium deposition compared to all other groups. Data plotted shows mean ± standard deviation (n=3). One-way ANOVA followed by Tukey post hoc analysis was performed and * indicates p<0.05, ** p<0.01 and *** p<0.001.

3.2 Comparison of BMP-2 protein functionality following transfection with modified BMP-2 plasmids on a 3D collagen hydroxyapatite scaffold

Having confirmed the osteoinductive effects of the BMP-2 plasmids in 2D monolayer, and therefore the ability of the CS nanoparticles to effectively deliver the plasmids to MSCs, we then tested the efficacy of the modified plasmids when incorporated into a gene-activated collagen hydroxyapatite (CHA) scaffold. Calcium deposition by cells was used as an indicator of MSC osteogenesis and was assessed using alizarin red staining at 28 days post-transfection while calcium content within the scaffolds was quantified at days 14 and 28. As with the 2D experiments, all cells were cultured in osteoinductive media with the exception of the untransfected GM group. The images shown in Figure 6 represent full scans of the scaffolds stained with alizarin red 28 days post-transfection. It is evident that there was more positive staining in the scaffolds containing BMP-2 plasmids but the CS-p_{CMV}BMP-2-Adv treated group appears to have stained more intensely for mineral. When calcium deposition was quantified (Figure 6), there was no significant difference in calcium content between untransfected cells in growth versus

osteoinductive media at each time point, reflecting the inherent osteoinductive nature of the collagen hydroxyapatite scaffold. However, the pBMP-2 treated groups deposited significantly more calcium than the control groups as is particularly evident at day 28 and again, CS-p_{CMV}BMP-2-Adv induced significantly more calcium deposition than all other groups.

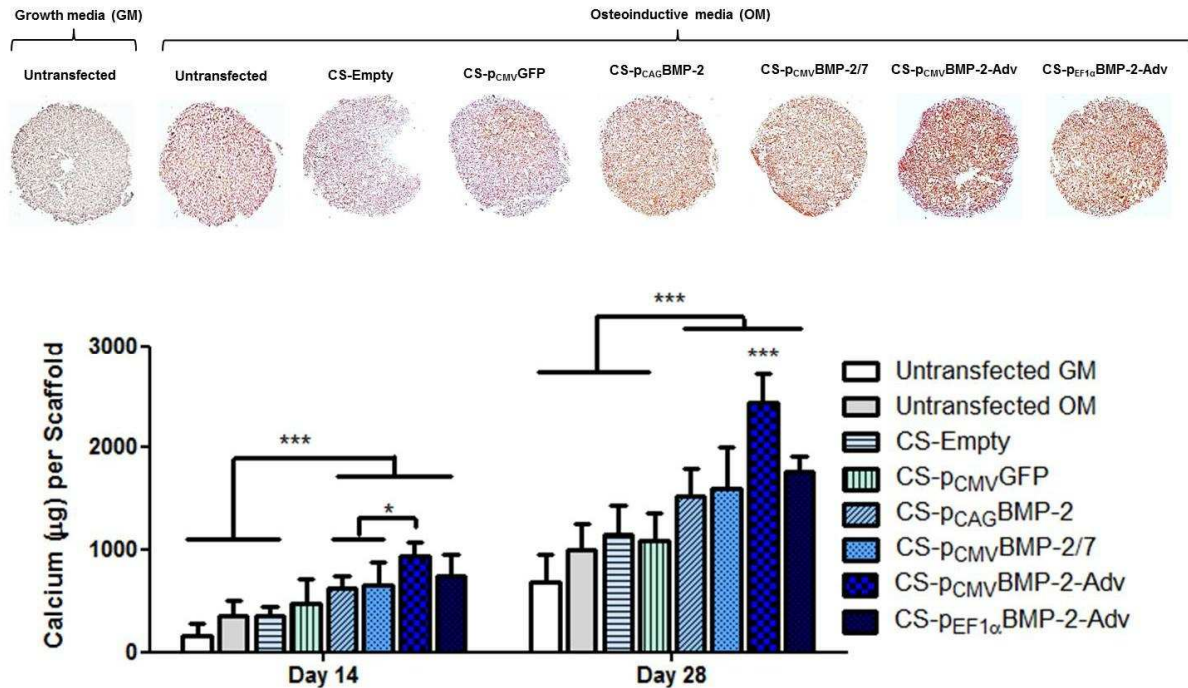


Figure 6. Effect of osteoinductive genes on MSC osteogenesis in 3D collagen hydroxyapatite scaffolds as measured by calcium deposition quantification. Untransfected cells in growth media (GM) and osteoinductive media (OM) were compared to cells treated with CS-empty, CS-p_{CMV}GFP, CS-p_{CAG}BMP-2, CS-p_{CMV}BMP-2/7, CS-p_{CMV}BMP-2-Adv and CS-p_{EF1α}BMP-2-Adv. Calcium deposition was quantified 14 and 28 days post-transfection. Mineral deposition (red) is seen in the 4x scans of each scaffold with more mineral evident in the BMP-2 treated groups over the controls. When calcium content was quantified, each condition induced cells to produce significantly more calcium than untransfected cells in growth media. Each variant of BMP-2 plasmid induced significantly more calcium deposition than controls without a BMP-2 plasmid. The CS-p_{CMV}BMP-2-Adv transfected group induced significantly higher levels of calcium deposition compared to all other groups. Data plotted shows mean \pm standard deviation (n=3). Two-way ANOVA followed by Bonferroni post hoc analysis was performed and * indicates $p < 0.05$ and *** $p < 0.001$.

3.3 Efficacy of gene-activated scaffold in accelerated repair of critical sized bone defects in vivo

From the in vitro testing in both 2D monolayer and in 3D gene-activated scaffolds, it was established that CS-p_{CMV}BMP-2-Adv was the most efficient at inducing MSC osteogenesis. We

then sought to investigate the efficacy of the gene-activated scaffold loaded with CS-p_{CMV}BMP-2-Adv in vivo in a critical sized calvarial defect (n=8) using an established rat model. To confirm that this plasmid is more efficient than p_{CAG}BMP-2, we also included CS-p_{CAG}BMP-2 activated scaffolds as a control (n=8) as well as a gene-free scaffold (n=8) and an untreated control (n=8). Recently published work has shown that gene-activated scaffolds are capable of accelerating bone formation [12, 17], thus an early time-point of 4 weeks was chosen for assessment. As 7mm represents a critical-sized defect, the lack of repair in the untreated group was expected (Figure 7A). The gene-free collagen hydroxyapatite scaffold has previously been shown to heal defects by 8-12 weeks [35, 38] so the low level of bone formation visible in Figure 7B at this early time-point was expected. The CS-p_{CAG}BMP-2 activated scaffold induced some de novo bone formation (Figure 7C); however, the CS-p_{CMV}BMP-2-Adv activated scaffold induced significantly more bone formation compared to all other groups (Figure 7D). When the new bone volume fraction was calculated, the CS-p_{CMV}BMP-2-Adv activated scaffold significantly enhanced bone formation (Figure 7E). Analysis of trabecular number (Figure 7F), trabecular thickness (Figure 7G) and trabecular spacing (Figure 7H) confirmed this result with a significantly higher number of trabeculae and thus less space between trabeculae in the animals treated with CS-p_{CMV}BMP-2-Adv activated scaffold compared to other groups. Trabecular thickness did not vary between groups.

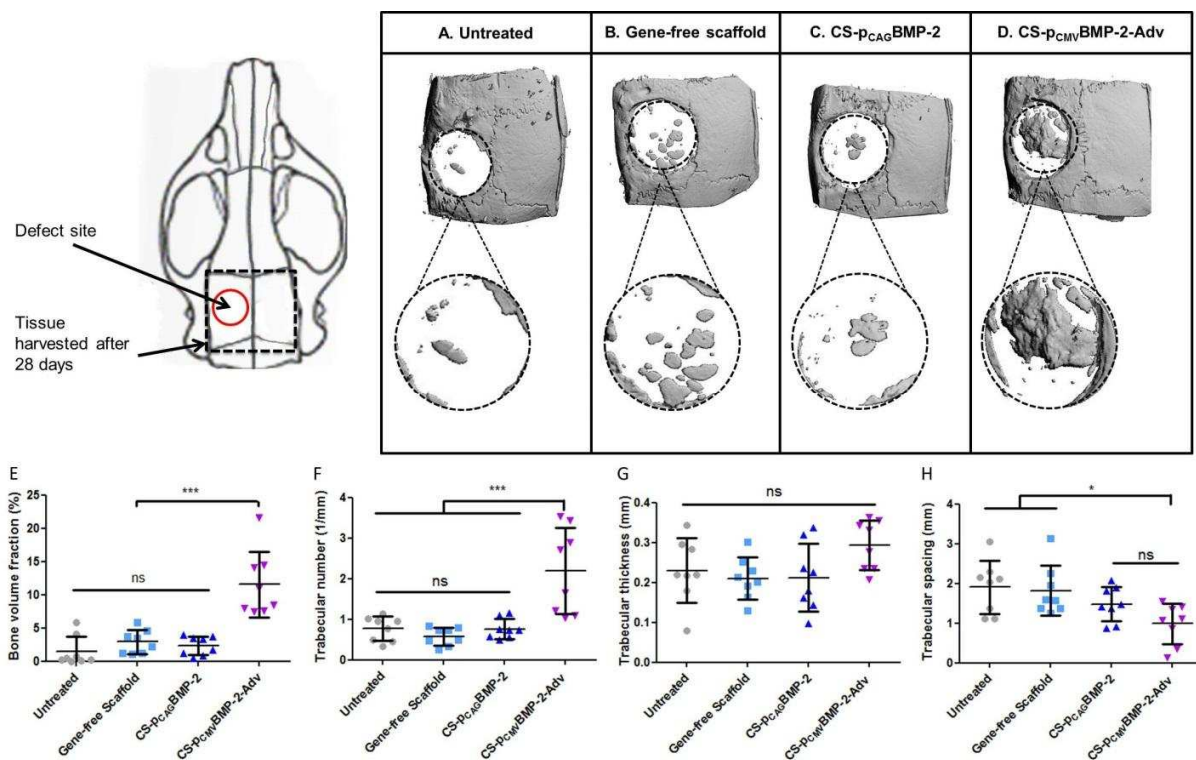


Figure 7. MicroCT analysis of bone repair in critical sized bone defects after 4 weeks. Critical size (7 mm) bone defects in the rat calvarium were A) untreated; or B) treated with a gene-free scaffold; C) a CS-p_{CAG}BMP-2 activated scaffold; or D) a CS-p_{CMV}BMP-2-Adv activated scaffold. Tissue was harvested 4 weeks post-implantation and new bone formation and quality was quantified using microCT. Representative reconstructed images show enhanced bone formation in the CS-p_{CMV}BMP-2-Adv scaffold group compared to control groups and when quantified, this was a significantly higher amount of new bone volume fraction (E). The quality of bone was also improved as indicated by trabecular number (F), trabecular thickness (G) and trabecular spacing (H). Data plotted shows mean ± standard deviation (n=8). One-way ANOVA followed by Tukey post hoc analysis was performed and * indicates p<0.05 and *** p<0.001.

Histological analysis of the calvarial tissue explants was consistent with the microCT results. When stained using H&E, the untreated defect explants had minimal new bone within the defect (pink) and consisted mainly of fibrous tissue (Figure 8A). More bone nucleation sites were evident in the gene-free and CS-p_{CAG}BMP-2 activated scaffolds but the majority of the tissue was fibrous in nature and the scaffold was visible (Figure 8B and C). In contrast, animals treated with the CS-p_{CMV}BMP-2-Adv activated scaffolds have large areas filled with new bone (Figure 8D). The area of new bone was quantified using an automated Image J programme based on pixel intensity (Figure 8E) and confirmed that the CS-p_{CMV}BMP-2-Adv activated scaffold induced significantly more bone formation compared to the other groups (p<0.05 to p<0.001). While there was no significant difference between the untreated, gene free scaffold and CS-p_{CAG}BMP-2 activated

scaffold groups, the results show a trend towards greater healing in treated versus untreated groups with untreated < gene-free scaffold < CS-p_{CAG}BMP-2 activated scaffold < CS-p_{CMV}BMP-2-Adv activated scaffold.

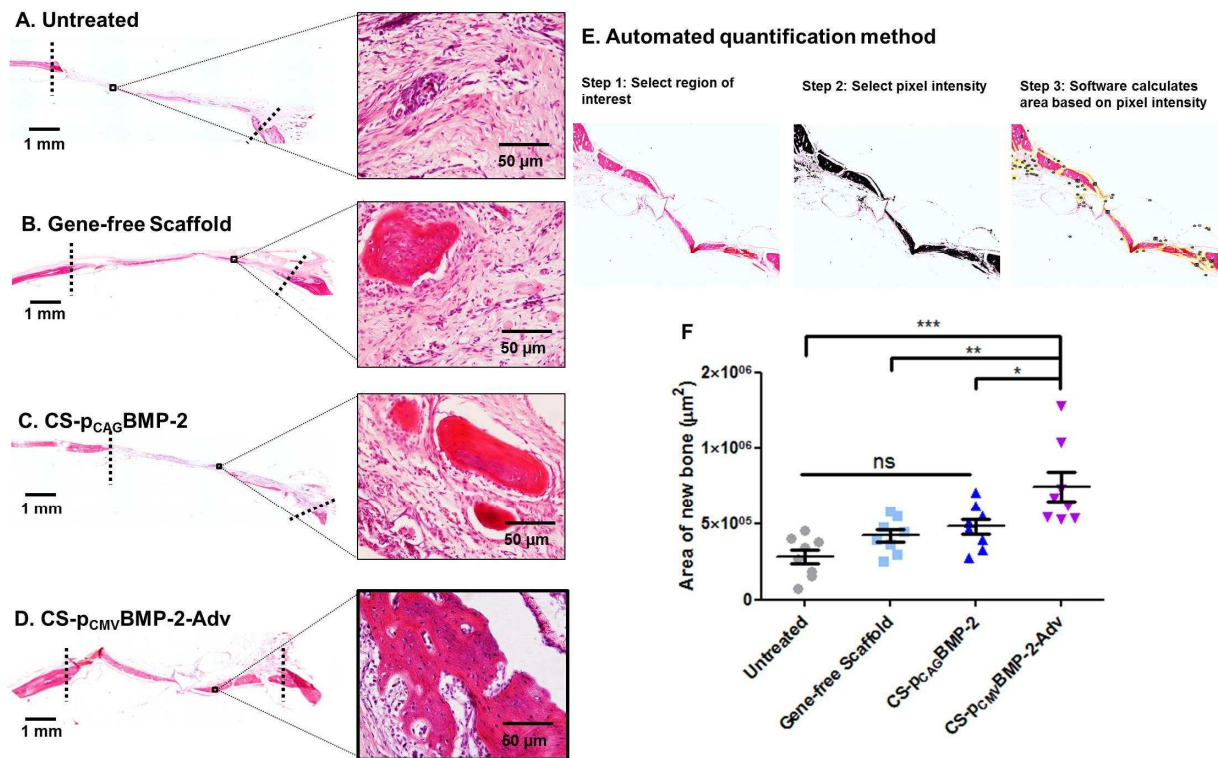


Figure 8. Histological analysis of bone repair in critical sized bone defects after 4 weeks. Representative H&E images of explants from calvarial defects at 4x and 20x magnification. H&E staining indicates bone in dark pink. A) Untreated; B) Gene-free scaffold; C) CS-p_{CAG}BMP-2 activated scaffold; D) CS-p_{CMV}BMP-2-Adv activated scaffold. Histomorphological analysis using an automated pixel intensity method (E) confirmed that the CS-p_{CMV}BMP-2-Adv activated scaffold significantly enhanced new bone formation compared to CS-p_{CAG}BMP-2 activated scaffolds and controls after 4 weeks (F). Data plotted shows mean ± standard deviation (n=8). One way ANOVA followed by Tukey post hoc analysis was performed and * indicates p<0.05, ** p<0.01 and *** p<0.001.

Immunohistochemistry was then performed to further analyse the process of bone formation of each of the groups. Col1a1 is a marker of early stage bone formation, being expressed by differentiating osteoprogenitor cells, while osteocalcin is a marker of late stage bone formation, being expressed by mature osteoblasts. Samples were stained using antibodies targeting Col1a1 (Figure 9, top panel) and osteocalcin (Figure 9, bottom panel) and clear differences were evident between groups. The explants from untreated animals (Figure 9A) did not stain positively for either

Col1a1 or osteocalcin, indicating that healing has not begun to any notable level. As this is a critical sized defect and with the lack of bone formation evident from microCT and histological analysis (Figures 7 and 8), this result is consistent with the rest of the study. There was positive staining for both markers in explants from animals treated with gene-free scaffolds (Figure 9B), CS-p_{CAG}BMP-2 activated scaffolds (Figure 9C) and CS-p_{CMV}BMP-2-Adv activated scaffolds (Figure 9D) although more positive staining is clearly evident in the latter. Using a similar automated Image J programme based on pixel intensity as described in Figure 8, positive staining was quantified. Animals treated with the gene-free scaffolds and CS-p_{CAG}BMP-2 activated scaffolds contained significantly more Col1a1 than untreated controls ($p < 0.05$ and $p < 0.01$ respectively) while in explants from animals treated with CS-p_{CMV}BMP-2-Adv activated scaffolds, Col1a1 staining was significantly higher than all other groups ($p < 0.001$) (Figure 9E). The same trend was evident when positive staining for osteocalcin was quantified although no significant differences were found between untreated, gene-free scaffolds and CS-p_{CAG}BMP-2 activated scaffolds. Explants from animals treated with CS-p_{CMV}BMP-2-Adv activated scaffolds had significantly more osteocalcin present compared to all other groups (Figure 9F).

Interestingly, there was more positive staining for Col1a1 versus osteocalcin in the gene-free scaffolds which may indicate that the bone healing process was at an earlier stage (Figure 9G). This result is consistent with the hypothesis that gene-activated scaffolds can accelerate bone healing as well as previous work which showed healing of defects after 8-12 weeks using the gene-free scaffold [35, 38]. Conversely, there was more positive staining for osteocalcin versus Col1a1 in the CS-p_{CMV}BMP-2-Adv activated scaffold which indicates that healing is at a later stage. Taken together, this study confirms that optimising the plasmid construct can translate to increased protein formation and confer enhanced therapeutic functionality to the gene-activated scaffold.

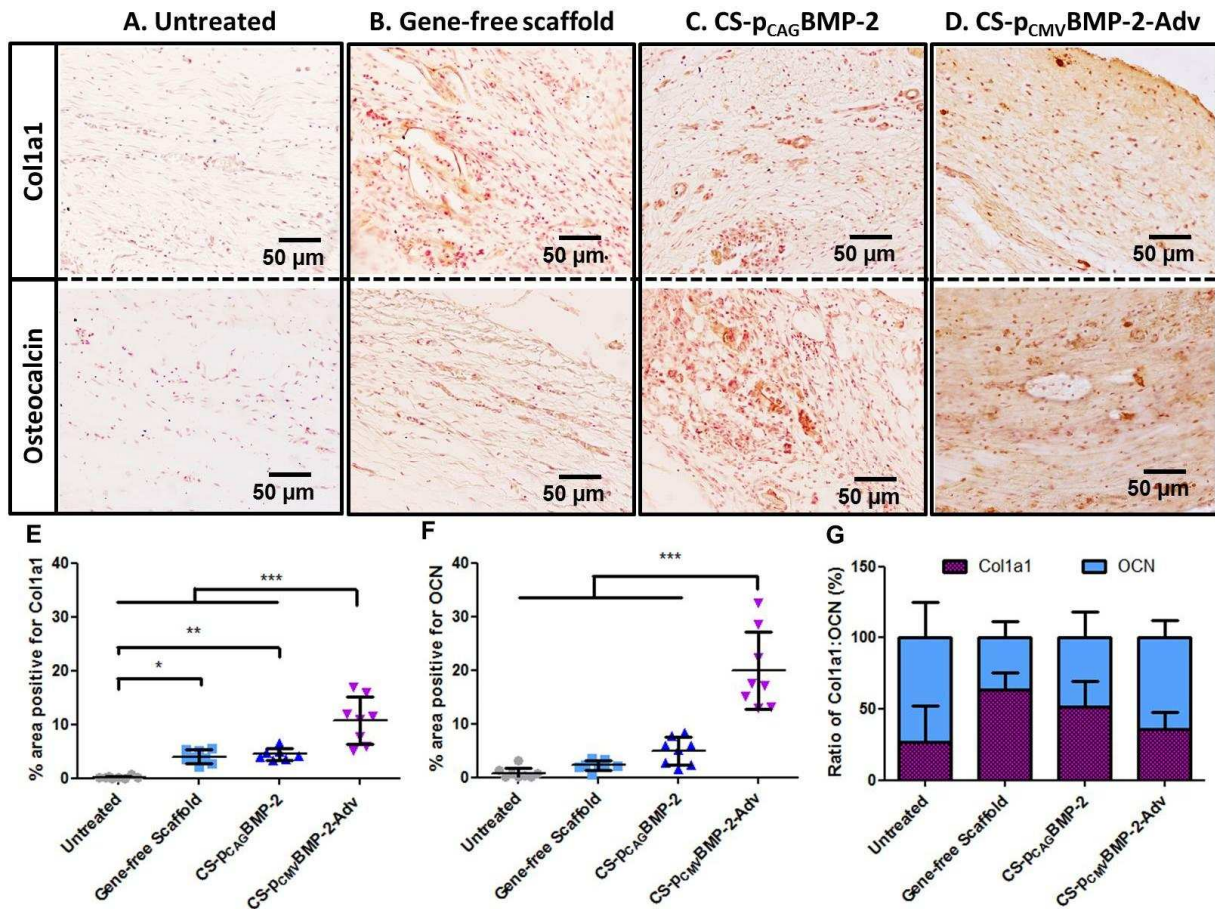


Figure 9. Immunohistochemistry analysis of bone repair in critical sized bone defect after 4 weeks. Representative images of explants from calvarial defects following immunohistochemical staining for Col1a1 (top row), an early stage marker of bone formation; and osteocalcin (bottom row), a late stage marker of bone formation at 20x magnification. A) Untreated; B) Gene-free scaffold; C) CS-p_{CAG}BMP-2 activated scaffold; D) CS-p_{CMV}BMP-2-Adv activated scaffold. Using an automated Image J programme based on pixel intensity, positive Col1a1 (E) and osteocalcin (F) staining was quantified showing significantly higher expression of bone matrix marker in CS-p_{CMV}BMP-2-Adv activated scaffolds. The ratio of Col1a1 positive staining versus osteocalcin positive staining indicates that the gene-activated scaffolds are accelerating bone repair (G). Data plotted shows mean \pm standard deviation (n=8). One way ANOVA followed by Tukey post hoc analysis was performed and * indicates $p < 0.05$, ** $p < 0.01$ and *** $p < 0.001$.

4. Discussion

BMP-2 delivery for bone repair has gained a lot of bad press due to adverse side effects reported following uncontrolled release of supraphysiological doses of recombinant protein [39, 40] which are required due to the short half-life of proteins in physiological conditions. Delivering genes encoding for the BMP-2 protein to host cells, instead of high doses of protein, circumvents the requirement for high dosing regimes as the cells begin to produce the required protein themselves. Gene delivery can be used to manipulate cells to produce therapeutic proteins themselves, thus controlling the release of physiological quantities of protein over time. The combination of gene delivery with tissue engineered biomaterial scaffolds allows for localised delivery of therapeutic to the defect site, thus limiting off-target side effects as well as providing a template for new tissue formation. The gene-activated scaffold system described in this paper is highly translatable as the base collagen hydroxyapatite scaffold has already undergone significant preclinical testing and is currently being used to treat defects in human patients [35, 36, 41-44]. The chitosan nanoparticles have been shown to be biocompatible and biodegradable unlike many polymer or lipid-based non-viral gene delivery vectors while maintaining a high transfection efficiency [45, 46]. Furthermore, previous work within our group has shown that the gene-activated scaffold has a good safety profile as the gene therapeutic was retained at the defect site, and was capable of accelerating bone repair in a rodent calvarial model of critical-sized bone defects when both p_{CAG}BMP-2 and p_{CMV}VEGF were delivered. However, the efficacy of a p_{CAG}BMP-2 gene-activated scaffold on its own was low in comparison [17]. The aim of this study was to investigate if improved BMP-2 plasmids could increase the efficiency of the gene-activated scaffold system and enhance bone repair in critical-sized defects.

The first objective of this study was to compare BMP-2 protein expression and functionality following transfection of MSCs with each of the BMP-2 plasmids. The use of a multi-cistronic plasmid was assessed to determine if heterodimeric BMP-2/7 expression enhanced bone formation over homodimeric BMP-2 expression [20]. The results show that p_{CMV}BMP-2/7 delivery did not enhance BMP-2 production over p_{CAG}BMP-2, however, this may be due to heterodimer formation rather than low expression of BMP-2 protein. This result is in agreement with previous studies which showed low BMP-2 production following transfection with the same p_{CMV}BMP-2/7 plasmid and may be due to an inability of the ELISA kit to detect the heterodimeric form of BMP-2/7 [20, 47]. Interestingly, the level of BMP-7 produced by pBMP-2/7 transfected cells was 5-fold higher than BMP-2 expression post-transfection with p_{CMV}BMP-2/7 (Supplementary Figure 1), in line with previous studies [19, 20] indicating that perhaps during post-transcriptional modifications,

the cells are producing more BMP-7 homodimers than BMP-2 homodimers or BMP-2/7 heterodimers. The p_{CMV}BMP-2-Adv and p_{EF1 α} BMP-2-Adv plasmids both contained a highly truncated artificial intron sequence and codon optimisation was performed to enhance transcription rate and translation of BMP-2 protein. Subsequently, the p_{CMV}BMP-2-Adv plasmid in particular induced faster and higher BMP-2 production by cells compared to p_{CAG}BMP-2, p_{CMV}BMP-2/7 and even p_{EF1 α} BMP-2-Adv reaching a peak of approximately 30 ng/mL at days 3 and 7. In contrast, here and in previous studies, peak protein expression was observed at day 10 post-transfection when p_{CAG}BMP-2 was used [17]. This indicates that the modifications to the BMP-2 gene carried out in the construction of the BMP-2-Advanced plasmids accelerated transcription and translation rates and the CMV promoter outperformed the EF1 α promoter. Most encouragingly, the level of protein production by MSCs transfected with the non-viral CS-p_{CMV}BMP-2-Adv was comparable to recently reported results delivering the BMP-2 gene using an adenoviral vector [48].

The BMP-2 protein produced by transfected cells was functional, with increased ALP activity by MSCs transfected with each BMP-2 encoding plasmid. Interestingly, ALP activity in cells transfected with both BMP-2-Advanced plasmids peaked at the earlier time-point of day 3 compared to the later peak at day 7 in cells transfected with p_{CAG}BMP-2 and p_{CMV}BMP-2/7. Calcium deposition was also highest in cells treated with p_{CMV}BMP-2-Adv. These results indicate that insertion of a highly truncated intron sequence into the BMP-2 gene, along with codon optimisation, resulted in more efficient transcription and translation of the BMP-2 gene leading to earlier and higher protein production and earlier osteogenic response by cells following transfection with p_{CMV}BMP-2-Adv.

The results from experiments carried out in 2D remained consistent when the plasmids were incorporated into collagen hydroxyapatite (CHA) scaffolds. The CHA scaffold was already shown to be osteoinductive due to the presence of hydroxyapatite crystals [41] but by loading the scaffold with CS nanoparticles carrying each BMP-2 plasmid, the osteoinductive potential of the scaffold was significantly enhanced. Alizarin red staining and calcium quantification showed that the CS-p_{CMV}BMP-2-Adv activated scaffold was the most osteoinductive with approximately 2500 μ g of calcium deposited by MSCs after 28 days. This result surpasses recent reports using the scaffold to deliver pBMP-2 with pVEGF [12, 17] as well as previous papers delivering rhBMP-2 [35, 36], highlighting the efficiency of the p_{CMV}BMP-2-Adv plasmid.

Due to the efficiency of the CS-p_{CMV}BMP-2-Adv activated scaffold in vitro, it was taken forward for implantation into a 7 mm calvarial defect in a rodent model and compared to CS-p_{CAG}BMP-2 activated scaffolds, gene-free scaffolds, and untreated controls. This model was chosen as it is well established within our group and allows for direct comparison between different scaffolds with and without additional therapeutics. Furthermore, as the calvarium is not load-bearing, variability between animals can be reduced although testing in large load-bearing defects such as the femur remains a requirement towards translation of these products. In the calvarial model, the 7mm defect is well established as being of a critical-size [49] and consistent with this, no healing was observed in the empty defect group. MicroCT and histomorphometry analysis at 4 weeks post-implantation showed that a significantly higher quantity of new bone was present within the defect in animals treated with the CS-p_{CMV}BMP-2-Adv activated scaffold compared to the other groups. The bone was also of higher quality to that of control groups as indicated by trabecular number. The results at this early time-point are impressive as most previous studies do not show a similar level of healing until 6-8 weeks post-implantation [50, 51]. Furthermore, the results are comparable to a recent study using chitosan films loaded with five times the dose of pBMP-2 (10 µg versus 2 µg used in this study) [52]. Another study using chitosan nanoparticles to deliver pBMP-2 within a chitosan hydrogel showed promising results although the defect was smaller (5 mm versus 7 mm in this study) and the methods used to determine new bone formation were qualitative rather than quantitative, making it difficult to draw comparisons [53].

Of most interest in this study was the difference in bone formation observed between the gene-activated scaffolds loaded with a BMP-2 plasmid versus the BMP-2-Advanced plasmid. The CS-p_{CAG}BMP-2 activated scaffold induced low levels of bone formation, no different to the gene-free scaffolds or indeed the untreated controls. While somewhat surprising, it may be that these treatments require more time to exert an osteoinductive effect. From previous work within our group, it was shown that the CHA scaffold can induce bridging of critical sized defects at 8 weeks post-implantation [38]. As was shown by the in vitro data, cells transfected with CS-p_{CAG}BMP-2 took longer to express BMP-2 protein, increase ALP activity, or deposit calcium compared to CS-p_{CMV}BMP-2-Adv transfected cells, therefore it is a reasonable assumption that the osteoinductive response of host cells to the CS-p_{CAG}BMP-2 activated scaffold might be delayed. To investigate further, immunohistochemistry was carried out looking at early (Col1a1) and late (osteocalcin) stage markers of bone formation [54]. As hypothesised, more active bone formation was promoted by the CS-p_{CMV}BMP-2-Adv scaffold compared to the other groups. However, there was more Col1a1 positive staining in the CS-p_{CAG}BMP-2 activated scaffold compared to the untreated control, indicating that there was some bone formation taking place. Interestingly, in the CS-

p_{CMV}BMP-2-Adv activated scaffold group, there was more osteocalcin present than Col1a1 which may indicate that the induced bone is at a more mature stage. Conversely, in the CS-p_{CAG}BMP-2 activated scaffold and gene-free scaffold treated animals, there was more Col1a1 than osteocalcin present indicating that bone formation was at an earlier stage. These results support the hypothesis that the BMP-2-Advanced plasmid can accelerate bone formation.

5. Conclusions

This study revealed that by using a modified BMP-2 plasmid, transcription and translation of the BMP-2 protein can be enhanced leading to earlier and higher levels of BMP-2 protein expression, increased ALP activity at an earlier time-point and enhanced calcium deposition. In vitro results were translated in vivo with significantly more bone formation observed at the early time-point of 4 weeks in defects treated with p_{CMV}BMP-2-Adv compared to the p_{CAG}BMP-2, and demonstrated that this result was due to delayed expression of lower levels of the bone markers Col1a1 and osteocalcin. Taken together, this study confirms that by optimising the plasmid construct, it is possible to accelerate and increase protein production and confer enhanced functionality to the gene-activated scaffold. This system essentially acts as a single-treatment therapeutic factory, inducing host cells which readily infiltrate the scaffold to produce BMP-2 at physiological levels, resulting in enhanced bone repair. Furthermore, the transient protein expression induced by the non-viral vector overcomes concerns associated with gene therapy and reduces the risk of off-target side effects. The gene-free collagen hydroxyapatite scaffold used in this study has already undergone rigorous in vitro and in vivo [31, 42, 55] testing and is now in human clinical use (marketed as HydroxyColl™ by SurgaColl Technologies) making this next generation gene-activated scaffold a highly translatable therapy for critical sized or non-union bone defects.

Acknowledgments

This work was funded by Science Foundation Ireland (SFI) Research Frontiers Programme (Grant No. 11/RFP/ENM/3053) and the Advanced Materials and Bioengineering Research (AMBER) Centre through SFI (SFI/12/RC/2278).

References

[1] S.D. Boden, T.A. Zdeblick, H.S. Sandhu, S.E. Heim, The use of rhBMP-2 in interbody fusion cages: definitive evidence of osteoinduction in humans: a preliminary report, *Spine*, 25 (2000) 376-381.

- [2] J.K. Burkus, M.F. Gornet, C.A. Dickman, T.A. Zdeblick, Anterior lumbar interbody fusion using rhBMP-2 with tapered interbody cages, *Clinical Spine Surgery*, 15 (2002) 337-349.
- [3] G.E. Friedlaender, C.R. Perry, J.D. Cole, S.D. Cook, G. Cierny, G.F. Muschler, G.A. Zych, J.H. Calhoun, A.J. LaForte, S. Yin, Osteogenic Protein-1 (Bone Morphogenetic Protein-7) in the Treatment of Tibial Nonunions : A Prospective, Randomized Clinical Trial Comparing rhOP-1 with Fresh Bone Autograft*, *JBJS*, 83 (2001) S151-S158.
- [4] A.R. Vaccaro, T. Patel, J. Fischgrund, D.G. Anderson, E. Truumees, H.N. Herkowitz, F. Phillips, A. Hilibrand, T.J. Albert, T. Wetzel, A pilot study evaluating the safety and efficacy of OP-1 Putty (rhBMP-7) as a replacement for iliac crest autograft in posterolateral lumbar arthrodesis for degenerative spondylolisthesis, *Spine*, 29 (2004) 1885-1892.
- [5] A.R. Vaccaro, J.P. Lawrence, T. Patel, L.D. Katz, D.G. Anderson, J.S. Fischgrund, J. Krop, M.G. Fehlings, D. Wong, The safety and efficacy of OP-1 (rhBMP-7) as a replacement for iliac crest autograft in posterolateral lumbar arthrodesis: a long-term (> 4 years) pivotal study, *Spine*, 33 (2008) 2850-2862.
- [6] T. Ratko, S. Belinson, D.J. Samson, C. Bonnell, K.M. Ziegler, N. Aronson, Bone morphogenetic protein: the state of the evidence of on-label and off-label use, (2010).
- [7] T.A. Einhorn, L.C. Gerstenfeld, Fracture healing: mechanisms and interventions, *Nature Reviews Rheumatology*, 11 (2015) 45-54.
- [8] R.M. Raftery, D.P. Walsh, I.M. Castaño, A. Heise, G.P. Duffy, S.-A. Cryan, F.J. O'Brien, Delivering Nucleic-Acid Based Nanomedicines on Biomaterial Scaffolds for Orthopedic Tissue Repair: Challenges, Progress and Future Perspectives, *Adv. Mater.*, 28 (2016) 5447-5469.
- [9] M. Kawai, K. Bessho, S. Kaihara, J. Sonobe, K. Oda, T. Iizuka, H. Maruyama, Ectopic bone formation by human bone morphogenetic protein-2 gene transfer to skeletal muscle using transcutaneous electroporation, *Human gene therapy*, 14 (2003) 1547-1556.
- [10] C.M. Curtin, G.M. Cunniffe, F.G. Lyons, K. Bessho, G.R. Dickson, G.P. Duffy, F.J. O'Brien, Innovative Collagen Nano-Hydroxyapatite Scaffolds Offer a Highly Efficient Non-Viral Gene Delivery Platform for Stem Cell-Mediated Bone Formation, *Adv. Mater.*, 24 (2012) 749-754.
- [11] E.G. Tierney, G.P. Duffy, A.J. Hibbitts, S.-A. Cryan, F.J. O'Brien, The development of non-viral gene-activated matrices for bone regeneration using polyethyleneimine (PEI) and collagen-based scaffolds, *J. Controlled Release*, 158 (2012) 304-311.
- [12] C.M. Curtin, E.G. Tierney, K. McSorley, S.-A. Cryan, G.P. Duffy, F.J. O'Brien, Combinatorial Gene Therapy Accelerates Bone Regeneration: Non-Viral Dual Delivery of VEGF and BMP2 in a Collagen-Nanohydroxyapatite Scaffold, *Adv. Healthcare Mater.*, 4 (2015) 223-227.
- [13] I.M. Castaño, C.M. Curtin, G. Shaw, J. Mary Murphy, G.P. Duffy, F.J. O'Brien, A novel collagen-nanohydroxyapatite microRNA-activated scaffold for tissue engineering applications capable of efficient delivery of both miR-mimics and antagomiRs to human mesenchymal stem cells, *J. Controlled Release*, 200 (2015) 42-51.
- [14] I. Mencía Castaño, C.M. Curtin, G.P. Duffy, F.J. O'Brien, Next generation bone tissue engineering: non-viral miR-133a inhibition using collagen-nanohydroxyapatite scaffolds rapidly enhances osteogenesis, *Scientific Reports*, 6 (2016) 27941.
- [15] K.A. Fitzgerald, J. Guo, R.M. Raftery, I.M. Castaño, C.M. Curtin, M. Gooding, R. Darcy, F.J. O'Brien, C.M. O'Driscoll, Nanoparticle-mediated siRNA delivery assessed in a 3D co-culture model simulating prostate cancer bone metastasis, *Int. J. Pharm.*, 511 (2016) 1058-1069.

- [16] R.M. Raftery, E.G. Tierney, C.M. Curtin, S.-A. Cryan, F.J. O'Brien, Development of a Gene-Activated Scaffold Platform for Tissue Engineering Applications Using Chitosan-pDNA Nanoparticles on Collagen-Based Scaffolds, *J. Controlled Release*, 210 (2015) 84-94.
- [17] R.M. Raftery, I.M. Castaño, G. Chen, B. Cavanagh, B. Quinn, C.M. Curtin, S.A. Cryan, F.J. O'Brien, Translating the role of osteogenic-angiogenic coupling in bone formation: Highly efficient chitosan-pDNA activated scaffolds can accelerate bone regeneration in critical-sized bone defects, *Biomaterials*, 149 (2017) 116-127.
- [18] M. Kawai, K. Bessho, H. Maruyama, J.-i. Miyazaki, T. Yamamoto, Simultaneous gene transfer of bone morphogenetic protein (BMP)-2 and BMP-7 by in vivo electroporation induces rapid bone formation and BMP-4 expression, *BMC musculoskeletal disorders*, 7 (2006) 62.
- [19] M. Kawai, H. Maruyama, K. Bessho, H. Yamamoto, J.-I. Miyazaki, T. Yamamoto, Simple strategy for bone regeneration with a BMP-2/7 gene expression cassette vector, *Biochem. Biophys. Res. Commun.*, 390 (2009) 1012-1017.
- [20] G. Feichtinger, A. Hofmann, K. Wassermann, A. Zimmermann, M. van Griensven, H. Redl, Constitutive and inducible co-expression systems for non-viral osteoinductive gene therapy, *Eur. Cell Mater.*, 27 (2014) 166-184.
- [21] A. Hacobian, D. Hercher, Pushing the right buttons: Improving efficacy of therapeutic DNA vectors, *Tissue Eng.*, (2017).
- [22] L. De Conti, M. Baralle, E. Buratti, Exon and intron definition in pre-mRNA splicing, *Wiley Interdisciplinary Reviews: RNA*, 4 (2013) 49-60.
- [23] M. Chorev, L. Carmel, The function of introns, *Frontiers in genetics*, 3 (2012).
- [24] N. Lane, W. Martin, The energetics of genome complexity, *Nature*, 467 (2010) 929.
- [25] W. Qian, J.-R. Yang, N.M. Pearson, C. Maclean, J. Zhang, Balanced codon usage optimizes eukaryotic translational efficiency, *PLoS genetics*, 8 (2012) e1002603.
- [26] J.R. Powell, E.N. Moriyama, Evolution of codon usage bias in *Drosophila*, *Proceedings of the National Academy of Sciences*, 94 (1997) 7784-7790.
- [27] N.J. Ward, S.M. Buckley, S.N. Waddington, T. VandenDriessche, M.K. Chuah, A.C. Nathwani, J. McIntosh, E.G. Tuddenham, C. Kinnon, A.J. Thrasher, Codon optimization of human factor VIII cDNAs leads to high-level expression, *Blood*, 117 (2011) 798-807.
- [28] A. Hacobian, K. Posa-Markaryan, S. Sperger, M. Stainer, D. Hercher, G. Feichtinger, C. Schuh, H. Redl, Improved osteogenic vector for non-viral gene therapy, *Eur. Cell Mater.*, 31 (2016) 191-204.
- [29] K.H. Khan, Gene Expression in Mammalian Cells and its Applications, *Advanced Pharmaceutical Bulletin*, 3 (2013) 257-263.
- [30] J.Y. Qin, L. Zhang, K.L. Clift, I. Hular, A.P. Xiang, B.-Z. Ren, B.T. Lahn, Systematic Comparison of Constitutive Promoters and the Doxycycline-Inducible Promoter, *PLoS ONE*, 5 (2010) e10611.
- [31] J. Gleeson, N. Plunkett, F. O'Brien, Addition of hydroxyapatite improves stiffness, interconnectivity and osteogenic potential of a highly porous collagen-based scaffold for bone tissue regeneration, *Eur. Cell Mater.*, 20 (2010) 218-230.
- [32] F.J. O'Brien, J.P. Gleeson, N. Plunkett, Collagen/hydroxyapatite composite scaffold, and process for the production thereof, in, *Google Patents*, 2013.
- [33] G.M. Cunniffe, C.M. Curtin, E.M. Thompson, G.R. Dickson, F.J. O'Brien, Content-Dependent Osteogenic Response of Nanohydroxyapatite: An in Vitro and in Vivo Assessment within Collagen-Based Scaffolds, *ACS Applied Materials & Interfaces*, 8 (2016) 23477-23488.

- [34] E.M. Thompson, A. Matsiko, D.J. Kelly, J.P. Gleeson, F.J. O'Brien, An Endochondral Ossification-Based Approach to Bone Repair: Chondrogenically Primed Mesenchymal Stem Cell-Laden Scaffolds Support Greater Repair of Critical-Sized Cranial Defects Than Osteogenically Stimulated Constructs In Vivo, *Tissue Engineering Part A*, 22 (2016) 556-567.
- [35] E. Quinlan, A. López-Noriega, E. Thompson, H.M. Kelly, S.A. Cryan, F.J. O'Brien, Development of collagen-hydroxyapatite scaffolds incorporating PLGA and alginate microparticles for the controlled delivery of rhBMP-2 for bone tissue engineering, *J. Controlled Release*, 198 (2015) 71-79.
- [36] E. Quinlan, E.M. Thompson, A. Matsiko, F.J. O'Brien, A. López-Noriega, Long-term controlled delivery of rhBMP-2 from collagen-hydroxyapatite scaffolds for superior bone tissue regeneration, *J. Controlled Release*, 207 (2015) 112-119.
- [37] C.A. Schneider, W.S. Rasband, K.W. Eliceiri, NIH Image to ImageJ: 25 years of image analysis, *Nature methods*, 9 (2012) 671-675.
- [38] F.G. Lyons, A.A. Al-Munajjed, S.M. Kieran, M.E. Toner, C.M. Murphy, G.P. Duffy, F.J. O'Brien, The healing of bony defects by cell-free collagen-based scaffolds compared to stem cell-seeded tissue engineered constructs, *Biomaterials*, 31 (2010) 9232-9243.
- [39] E.J. Carragee, E.L. Hurwitz, B.K. Weiner, A critical review of recombinant human bone morphogenetic protein-2 trials in spinal surgery: emerging safety concerns and lessons learned, *The Spine Journal*, 11 (2011) 471-491.
- [40] L.B. Shields, G.H. Raque, S.D. Glassman, M. Campbell, T. Vitaz, J. Harpring, C.B. Shields, Adverse effects associated with high-dose recombinant human bone morphogenetic protein-2 use in anterior cervical spine fusion, *Spine*, 31 (2006) 542-547.
- [41] F.G. Lyons, J.P. Gleeson, S. Partap, K. Coghlan, F.J. O'Brien, Novel Microhydroxyapatite Particles in a Collagen Scaffold: A Bioactive Bone Void Filler?, *Clinical orthopaedics and related research*, 472 (2014) 1318-1328.
- [42] F. David, T.J. Levingstone, W. Schneeweiss, M. Swarte, H. Jahns, J.P. Gleeson, F.J. O'Brien, Enhanced bone healing using collagen-hydroxyapatite scaffold implantation in the treatment of a large multiloculated mandibular aneurysmal bone cyst in a thoroughbred filly, *Journal of tissue engineering and regenerative medicine*, 9 (2015) 1193-1199.
- [43] E. Quinlan, A. López-Noriega, E.M. Thompson, A. Hibbitts, S.A. Cryan, F.J. O'Brien, Controlled release of vascular endothelial growth factor from spray-dried alginate microparticles in collagen-hydroxyapatite scaffolds for promoting vascularization and bone repair, *Journal of tissue engineering and regenerative medicine*, (2015) n/a-n/a.
- [44] E. Quinlan, E.M. Thompson, A. Matsiko, F.J. O'Brien, A. López-Noriega, Functionalization of a collagen-hydroxyapatite scaffold with osteostatin to facilitate enhanced bone regeneration, *Adv. Healthcare Mater.*, 4 (2015) 2649-2656.
- [45] C. Brunot, L. Ponsonnet, C. Lagneau, P. Farge, C. Picart, B. Grosgeat, Cytotoxicity of polyethyleneimine (PEI), precursor base layer of polyelectrolyte multilayer films, *Biomaterials*, 28 (2007) 632-640.
- [46] H. Lv, S. Zhang, B. Wang, S. Cui, J. Yan, Toxicity of cationic lipids and cationic polymers in gene delivery, *J. Controlled Release*, 114 (2006) 100-109.
- [47] T. Kaito, J. Johnson, J. Ellerman, H. Tian, M. Aydogan, M. Chatsrinopkun, S. Ngo, C. Choi, J.C. Wang, Synergistic effect of bone morphogenetic proteins 2 and 7 by ex vivo gene therapy in a rat spinal fusion model, *The Journal of Bone & Joint Surgery*, 95 (2013) 1612-1619.
- [48] B. Ren, V.M. Betz, C. Thirion, M. Salomon, V. Jansson, P.E. Müller, O.B. Betz, Gene-activated tissue grafts for sustained bone morphogenetic protein-2 delivery and bone engineering:

Is muscle with fascia superior to muscle and fat?, *Journal of Tissue Engineering and Regenerative Medicine*, epub ahead of print (2017) n/a-n/a.

[49] P.P. Spicer, J.D. Kretlow, S. Young, J.A. Jansen, F.K. Kasper, A.G. Mikos, Evaluation of bone regeneration using the rat critical size calvarial defect, *Nature protocols*, 7 (2012) 1918-1929.

[50] M. Endo, S. Kuroda, H. Kondo, Y. Maruoka, K. Ohya, S. Kasugai, Bone regeneration by modified gene-activated matrix: effectiveness in segmental tibial defects in rats, *Tissue Eng.*, 12 (2006) 489-497.

[51] F. Liu, R.M. Porter, J. Wells, V. Glatt, C. Pilapil, C.H. Evans, Evaluation of BMP-2 gene-activated muscle grafts for cranial defect repair, *Journal of Orthopaedic Research*, 30 (2012) 1095-1102.

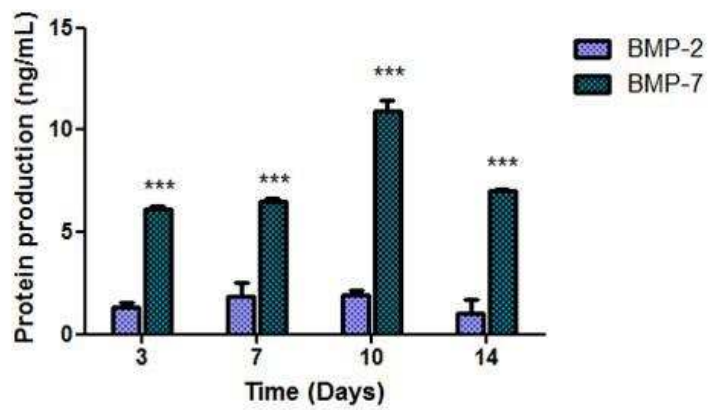
[52] J. Li, J. Lin, W. Yu, X. Song, Q. Hu, J.-H. Xu, H. Wang, C. Mehl, BMP-2 plasmid DNA-loaded chitosan films – A new strategy for bone engineering, *Journal of Cranio-Maxillofacial Surgery*, (2017).

[53] H. Li, Q. Ji, X. Chen, Y. Sun, Q. Xu, P. Deng, F. Hu, J. Yang, Accelerated bony defect healing based on chitosan thermosensitive hydrogel scaffolds embedded with chitosan nanoparticles for the delivery of BMP2 plasmid DNA, *Journal of Biomedical Materials Research Part A*, 105 (2017) 265-273.

[54] V.S. Salazar, L.W. Gamer, V. Rosen, BMP signalling in skeletal development, disease and repair, *Nat Rev Endocrinol*, 12 (2016) 203-221.

[55] J.P. Gleeson, T.J. Levingstone, F.J. O'brien, Layered scaffold suitable for osteochondral repair, in, *Google Patents*, 2010.

Supplementary Figures



Supplementary Figure 1. Protein production by cells transfected with pBMP-2/7. BMP-2 and BMP-7 protein production as monitored by ELISA at day 3, 7, 10 and 14 post-transfection with CS-p_{CMV}BMP-2/7. BMP-7 production was approximately 5-fold higher than BMP-2 production. Data plotted represents mean \pm SD where n=3 and *** represents $p < 0.001$.